Multi-Instrument Observations of Geomagnetic Storms in the Arctic Ionosphere

Tibor Durgonics*[1,2], Attila Komjathy[1,3], Olga Verkhoglyadova[1], Esayas B. Shume[1,4], Hans-Henrik Benzon[2], Anthony J. Mannucci[1], Mark D. Butala[5], Per Høeg[2], and Richard B. Langley[3]

***e-mail: tibdu@space.dtu.dk**

1 NASA Jet Propulsion Laboratory, Pasadena, CA, USA.

2 Technical University of Denmark, National Space Institute (DTU Space), Kongens Lyngby, Denmark

3 Dept. of Geodesy and Geomatics Engineering, University of New Brunswick, N.B., Canada

4 Astronomy Department, Caltech, Pasadena, CA, USA

5 University of Illinois at Urbana-Champaign, Champaign, IL, USA

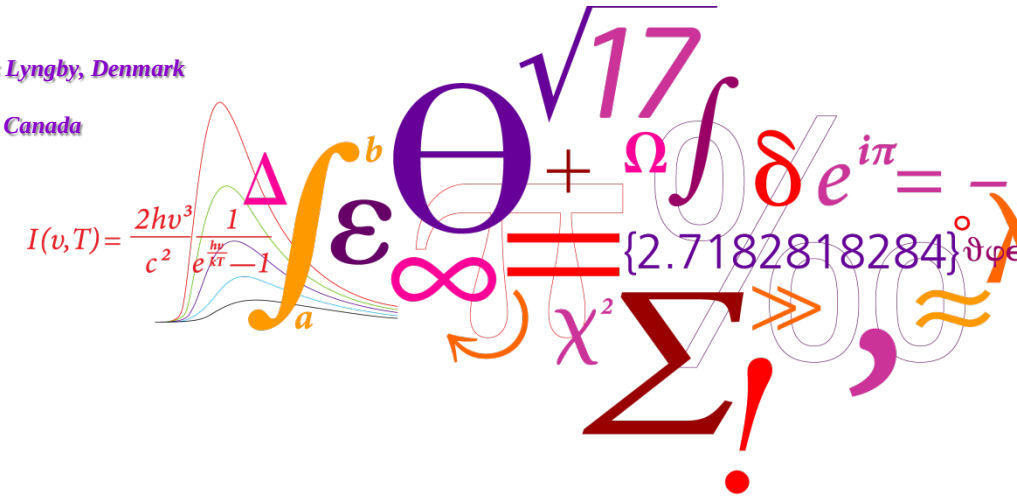

DTU Space
National Space Institute

Outline

- We present a multi-instrumented approach for the analysis of the Arctic ionosphere during the **19 February 2014** highly complex, multiphase **geomagnetic storm**.

- The geomagnetic storm was the result of two powerful Earth-directed coronal mass ejections (CMEs).

- In this talk we focus on this specific case study but all the significant similar events in 2014 exhibited similar development.

- Based on the **multiple instrument observation approach** and analyses technique we present the **physical processes that may be responsible for ionospheric storm development** in the northern high-latitudes.

Motivation and Background – Arctic Region

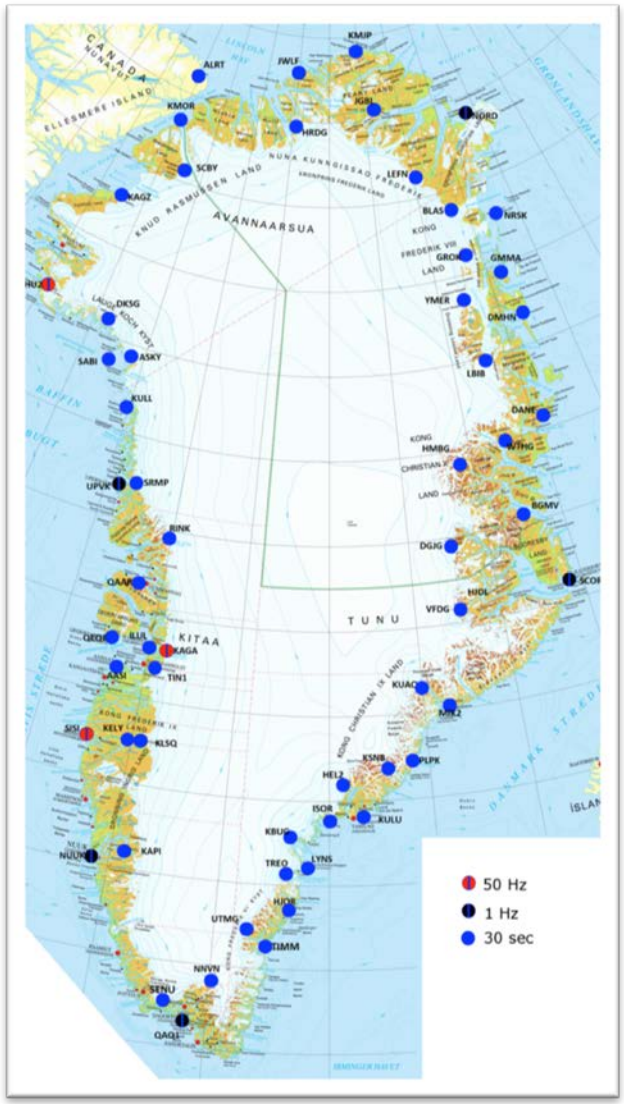

Motivation and Background – Arctic Ionosphere

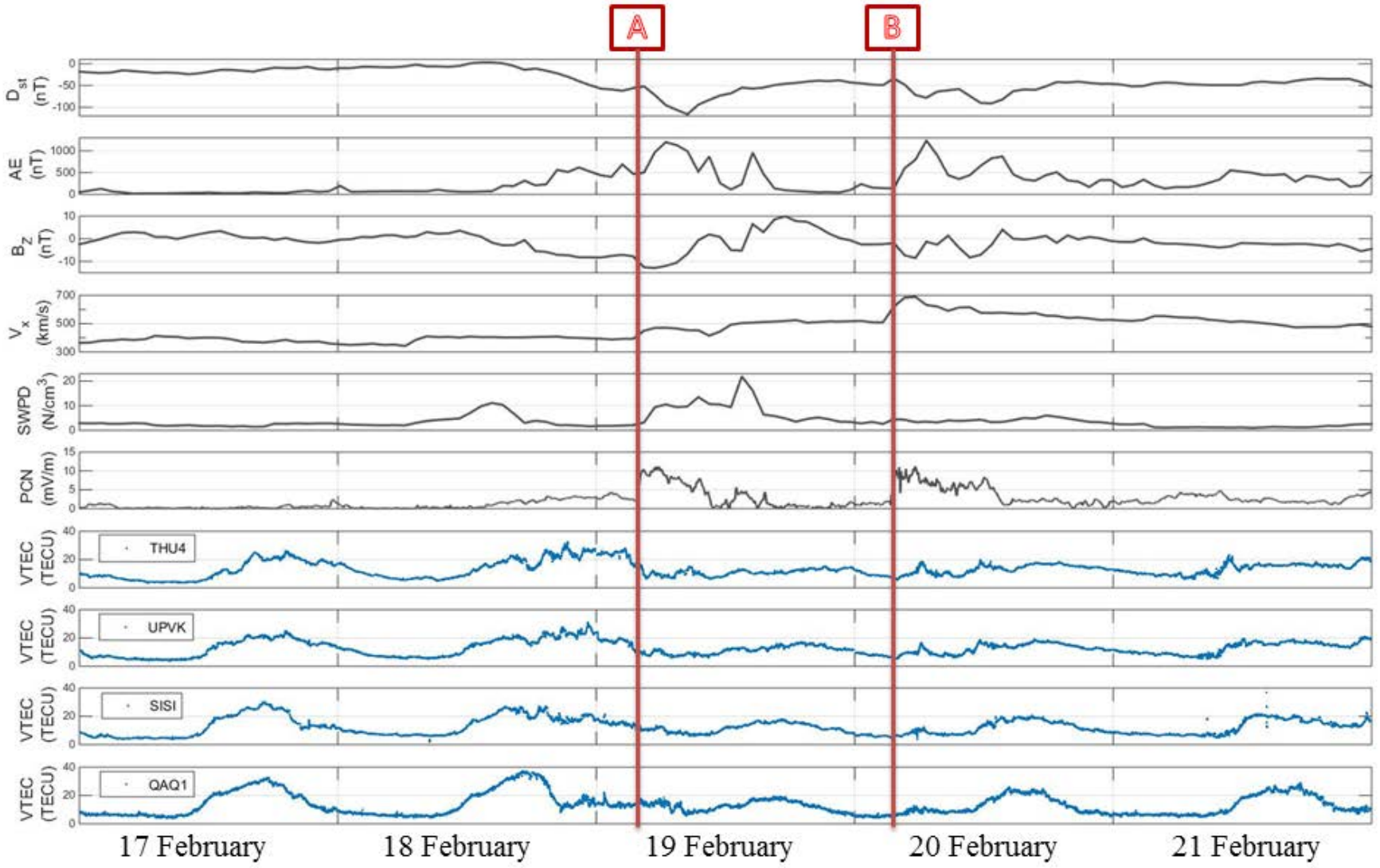

Motivation and Background – N_e depletion

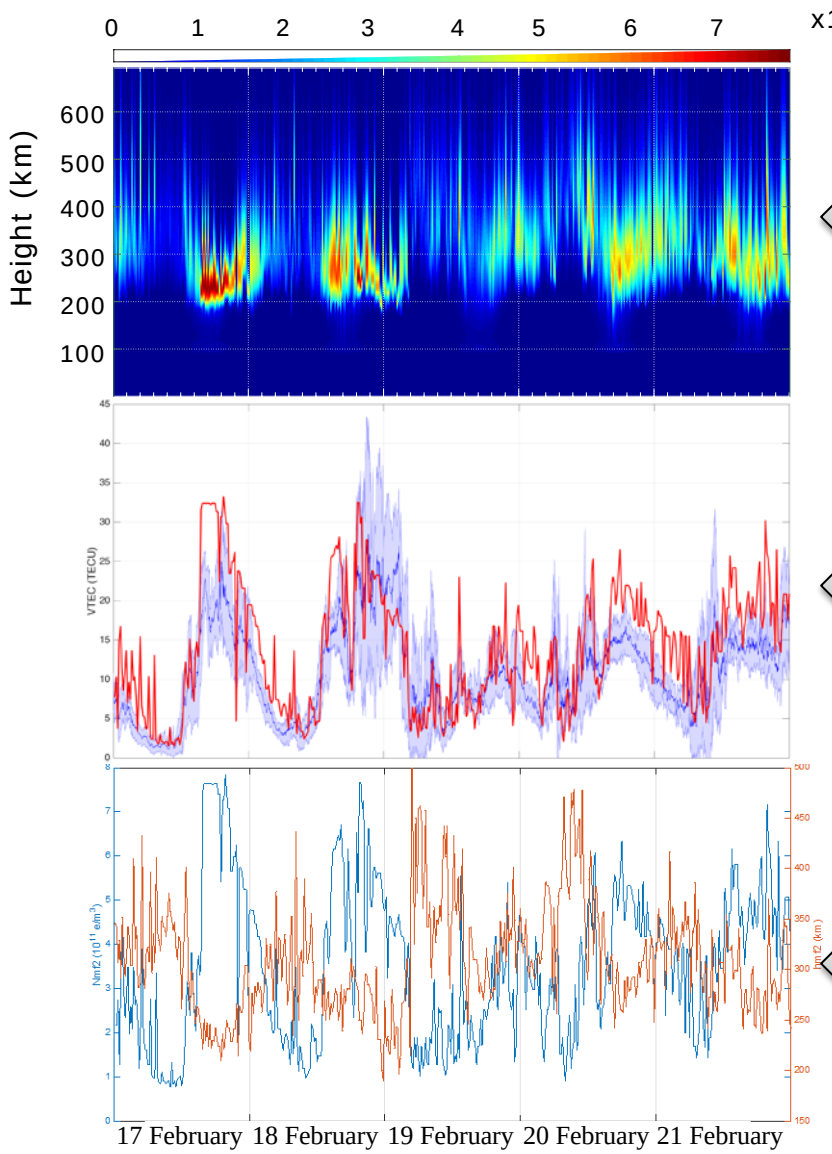

Ionosonde-derived N_e profiles (height [km])

VTEC vs. **integrated N_e**

NmF2 vs. **HmF2**

Instruments and Techniques
GNET – The Greenland GNSS Ground-Station Network

Instruments and Techniques
GNET – The Greenland GNSS ground-station network

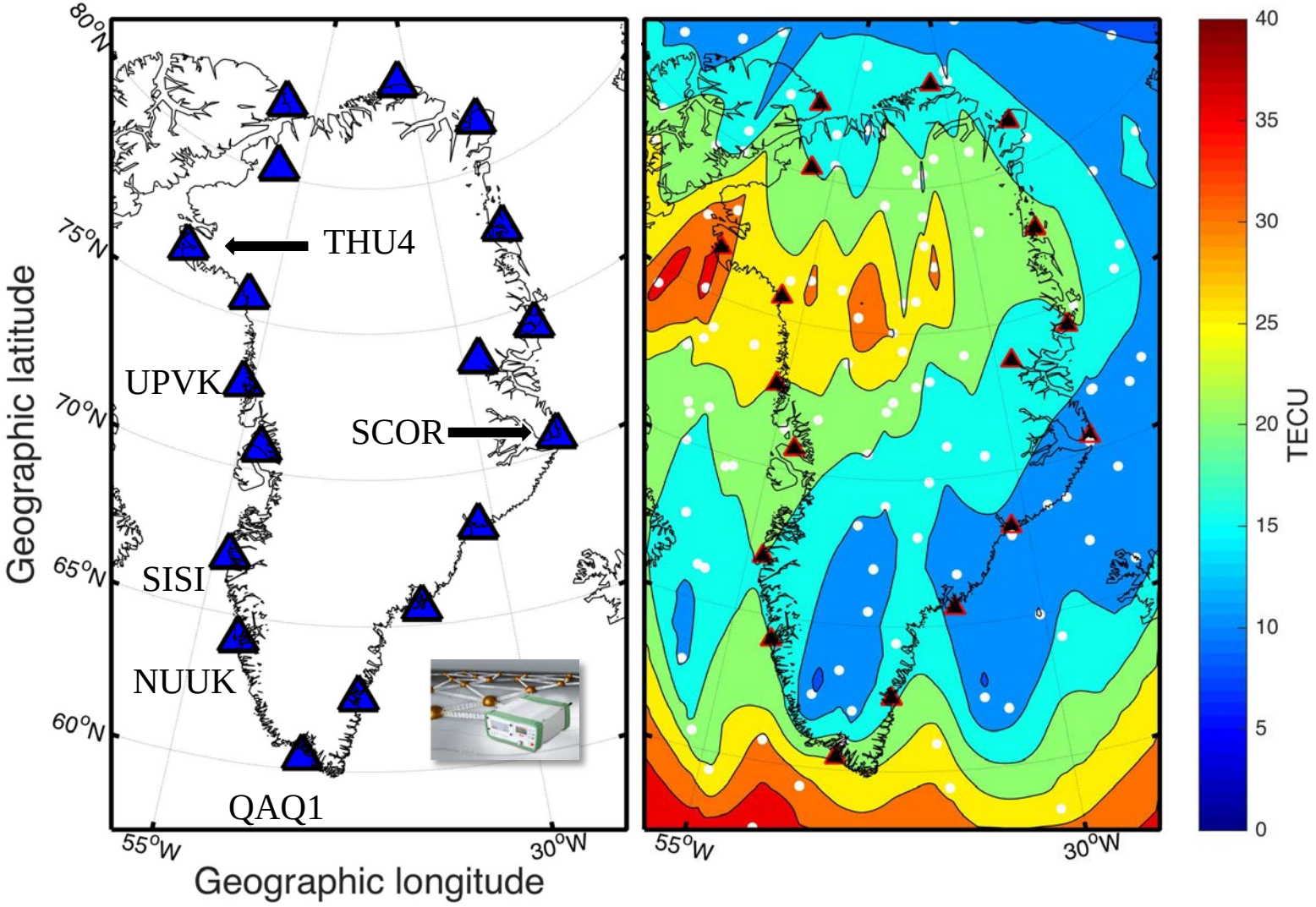

Instruments and Techniques - SuperDARN

- **Super Dual Auroral Radar Network**
- Primarily used to map high-latitude plasma convection in the F region of the ionosphere
- Possible comparison with SuperDARN convection maps

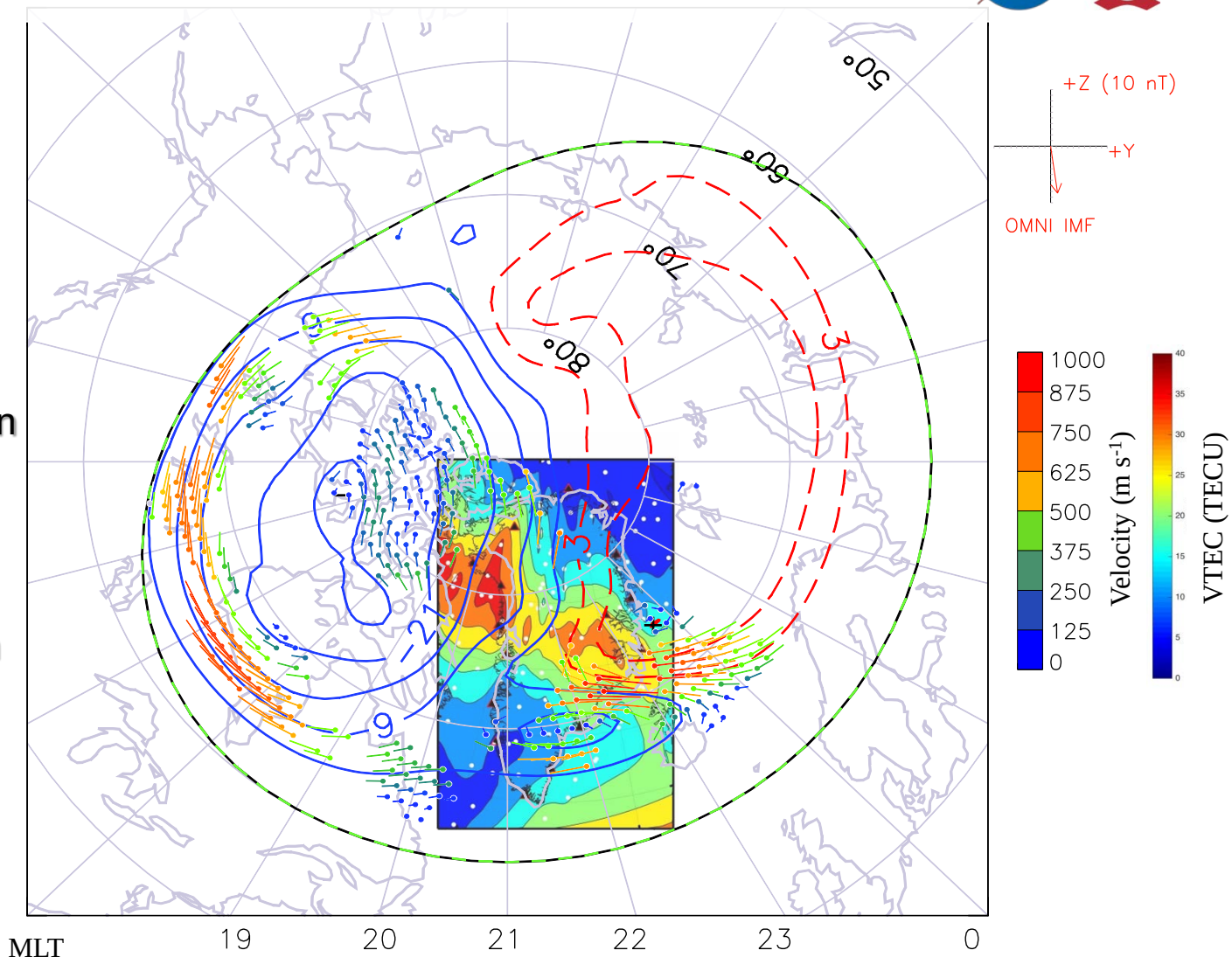

Instruments and Techniques – GNSS-TEC and ROTI

Rate of TEC (ROT) and **ROTI** can be computed from the same data source as TEC using $L_{1,2}$, the corresponding wavelengths ($\lambda_{1,2}$) and frequencies ($f_{1,2}$) followed by evaluating the following equations [Pi et al., 2013],

$$ROT(t) = \frac{L_I(t) - L_I(t - \Delta t)}{40.3 \times 10^{16} \times \Delta t \left(\frac{1}{f_1^2} - \frac{1}{f_2^2}\right)}$$

where ROT is in *TECU/min* units, t and Δt are the time at any epoch and the sampling rate in minutes respectively. ROTI is defined as the de-trended standard deviation of ROT over N epochs, i.e.,

$$ROTI(t) = \sqrt{\frac{1}{N}\sum_{t-N}^{t}(ROT(t - N) - \overline{ROT})^2}$$

which is calculated using a 1-minute running window.

Instruments and Techniques – GNSS-TEC and ROTI

- Published studies established that **ROTI, σ_φ, and S_4** (when S_4 is not suppressed) **are typically well-correlated**, but their magnitudes show a non-linear relationship [Pi et al., 2013].

- In the Arctic region high-speed (~1000 m/s) polar plasma convection plays an important role in **suppressing S_4 due to the Fresnel filtering** effect.

- Phase scintillation **does not depend on Fresnel zone size** [Gherm et al., 1995].

Why ROTI?

- GNET consists of geodetic GNSS receivers that are **producing data well-suited for ROTI** calculation.

- For computational reasons it is **not susceptible to clock/oscillator errors** and drifts.

- Directly **measures ionospheric TEC irregularities** ($L_1 - L_2$).

Results – GNSS-TEC and ROTI

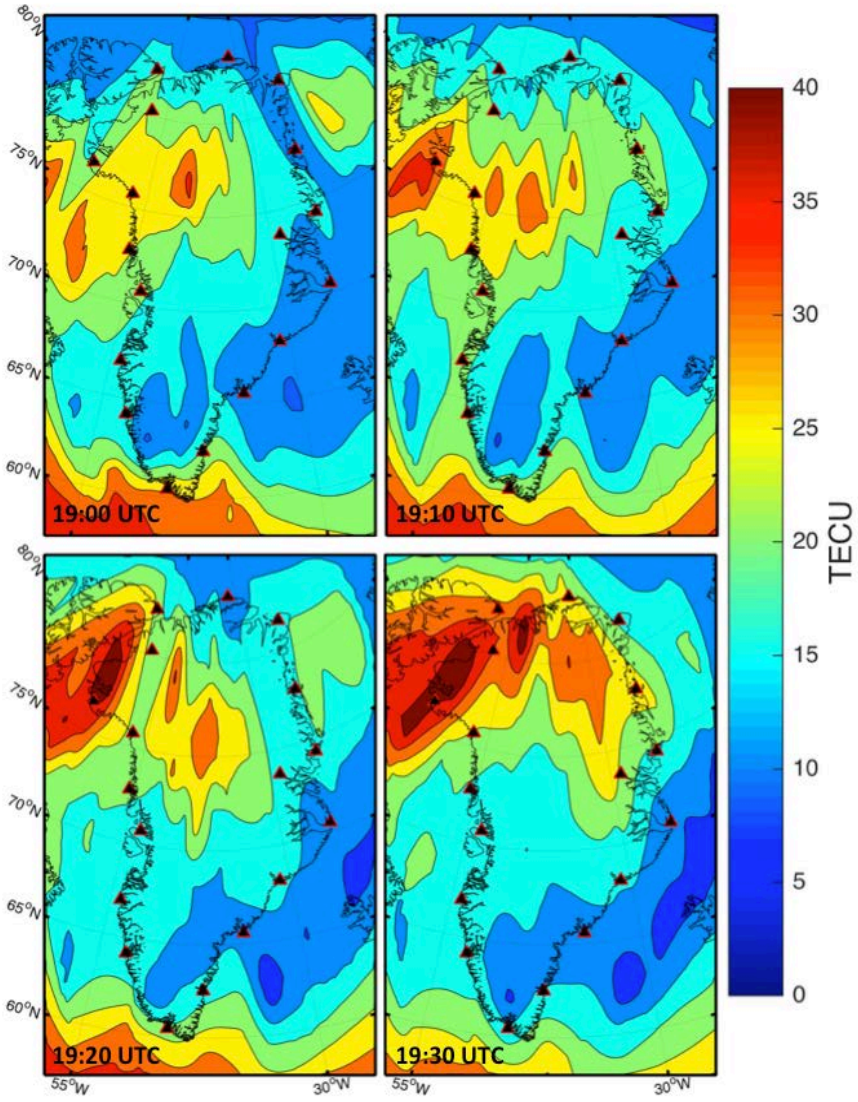

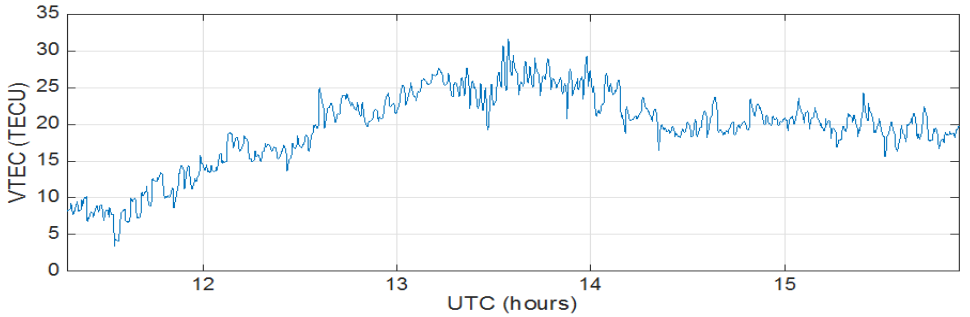

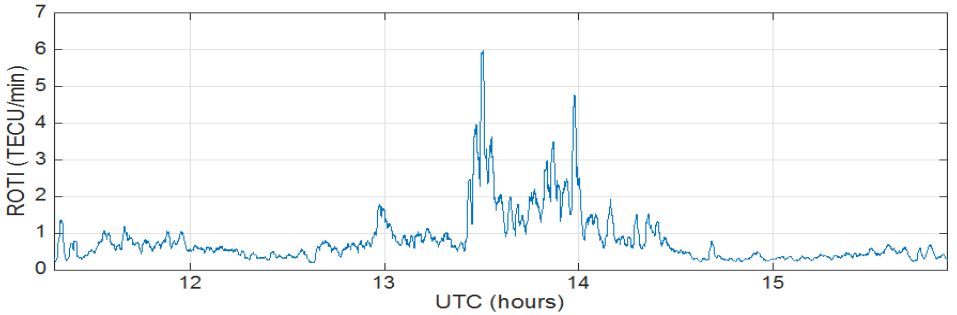

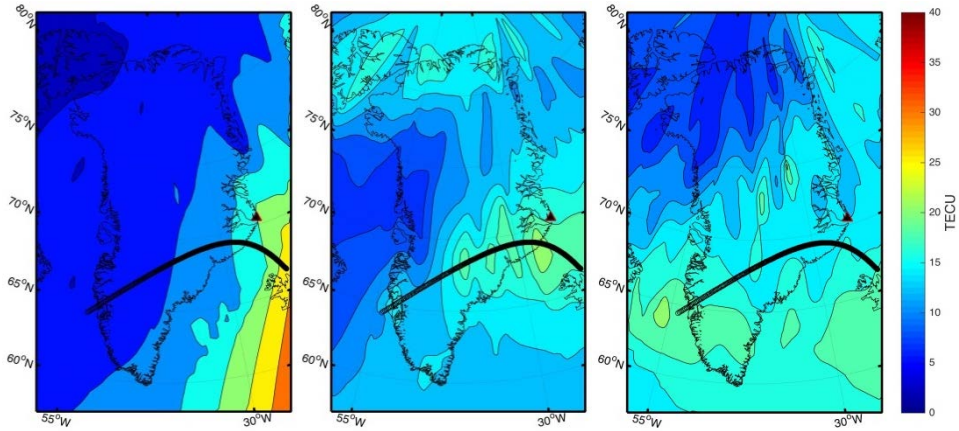

VTEC Observations

- 2014 February 19 Geomagnetic Storm - VTEC

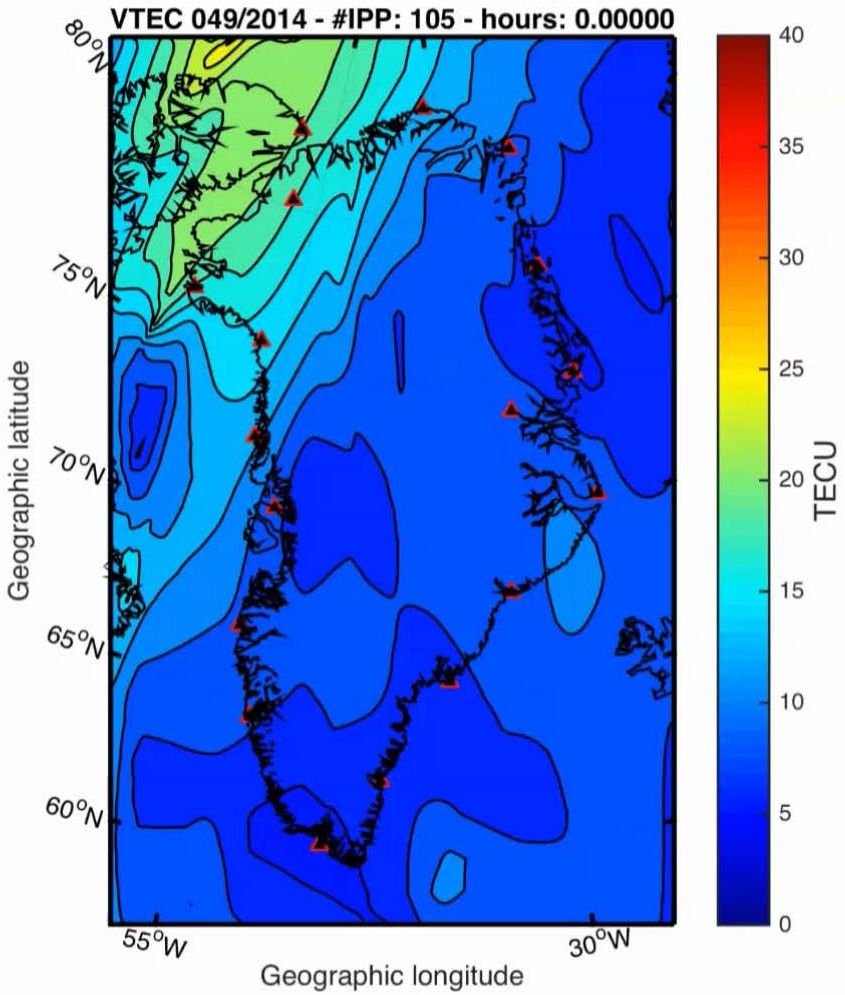

Results – Local Magnetic Measurements

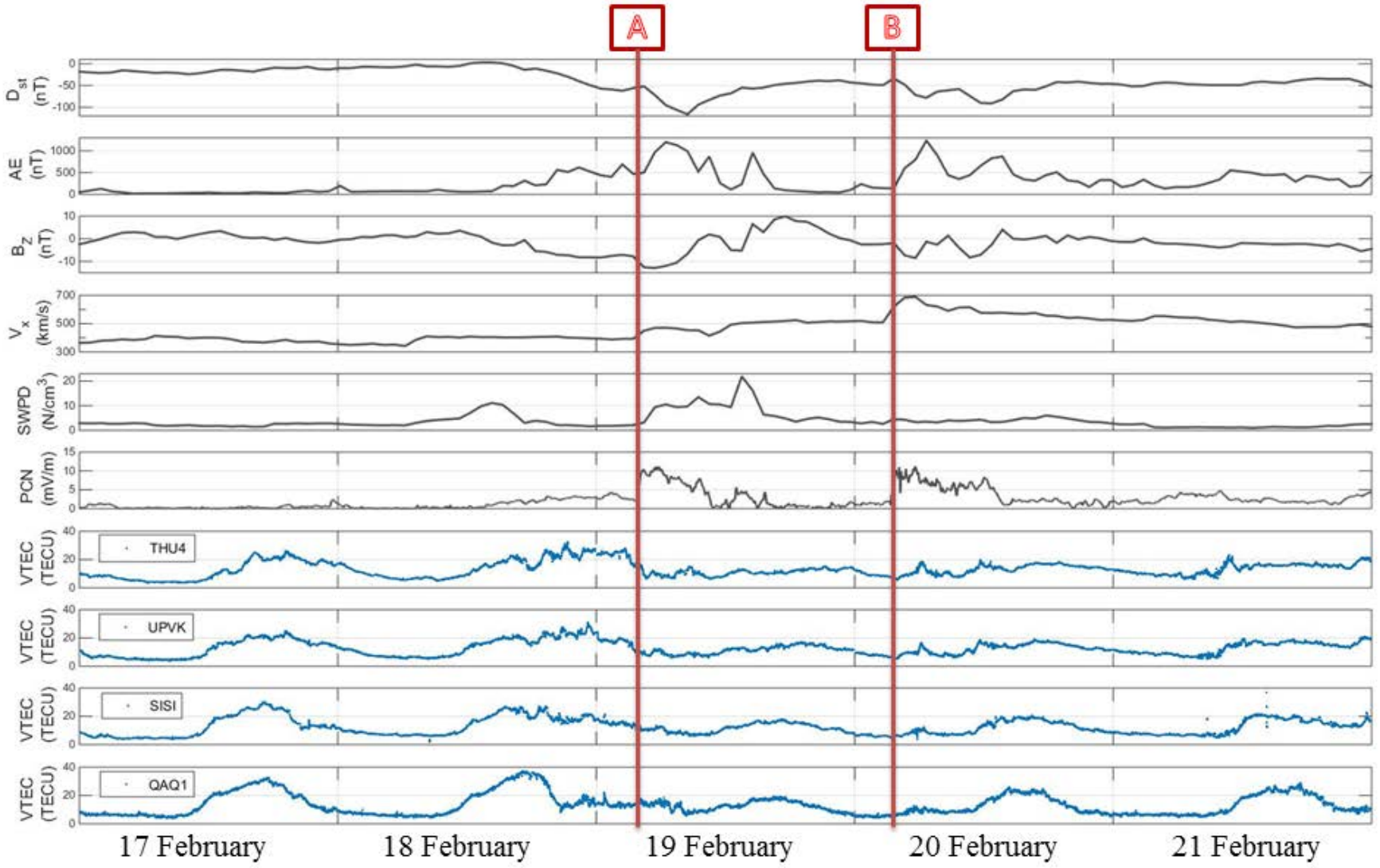

Results - GUVI

- O/N_2 ratio maps demonstrating composition changes during the six days we investigated. The first CME hit on 19 February and the second on 20 February.

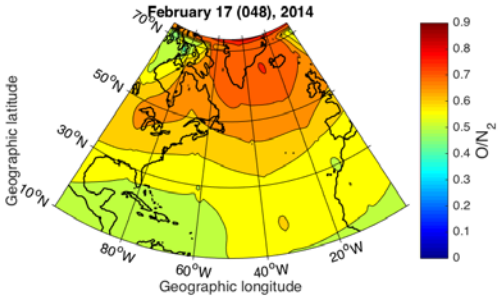

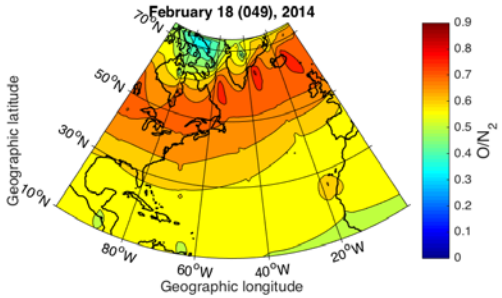

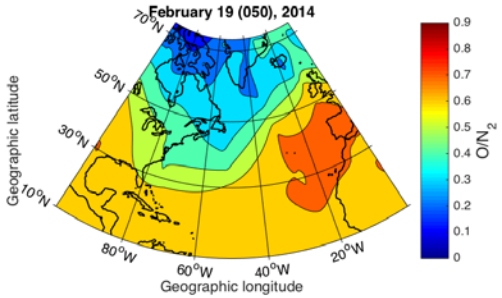

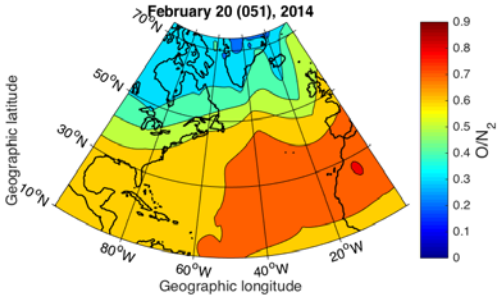

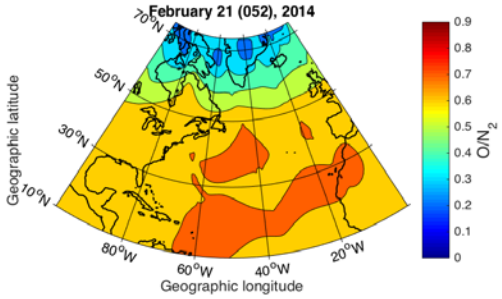

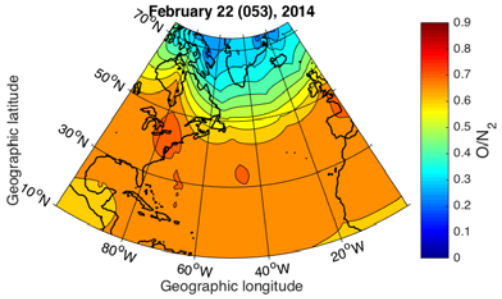

CASSIOPE
(CAScade, Smallsat and IOnospheric Polar Explorer)

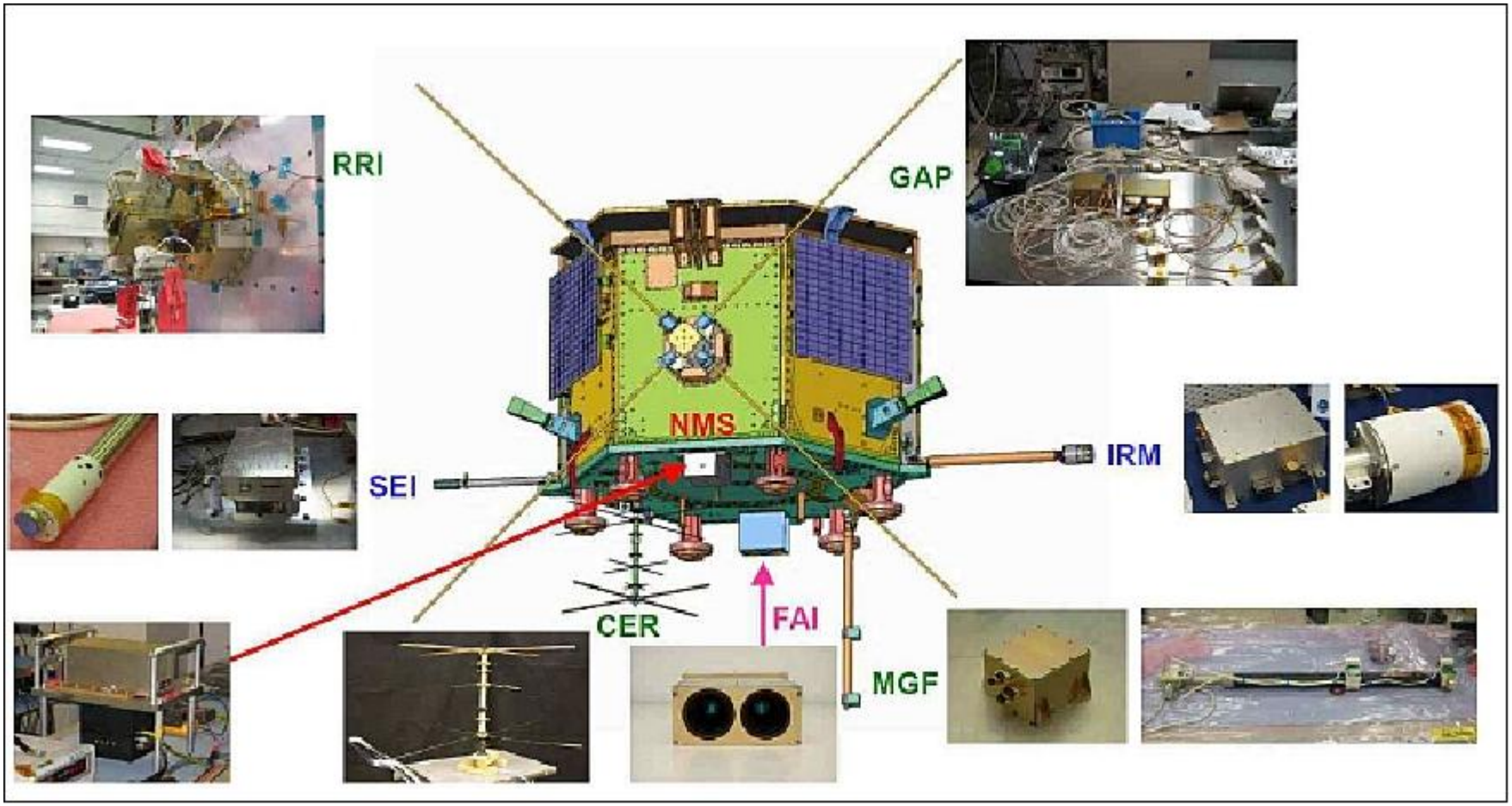

- **Imaging and Rapid Scanning Ion Mass Spectrometer (IRM)**, measuring the three-dimensional distribution of ions

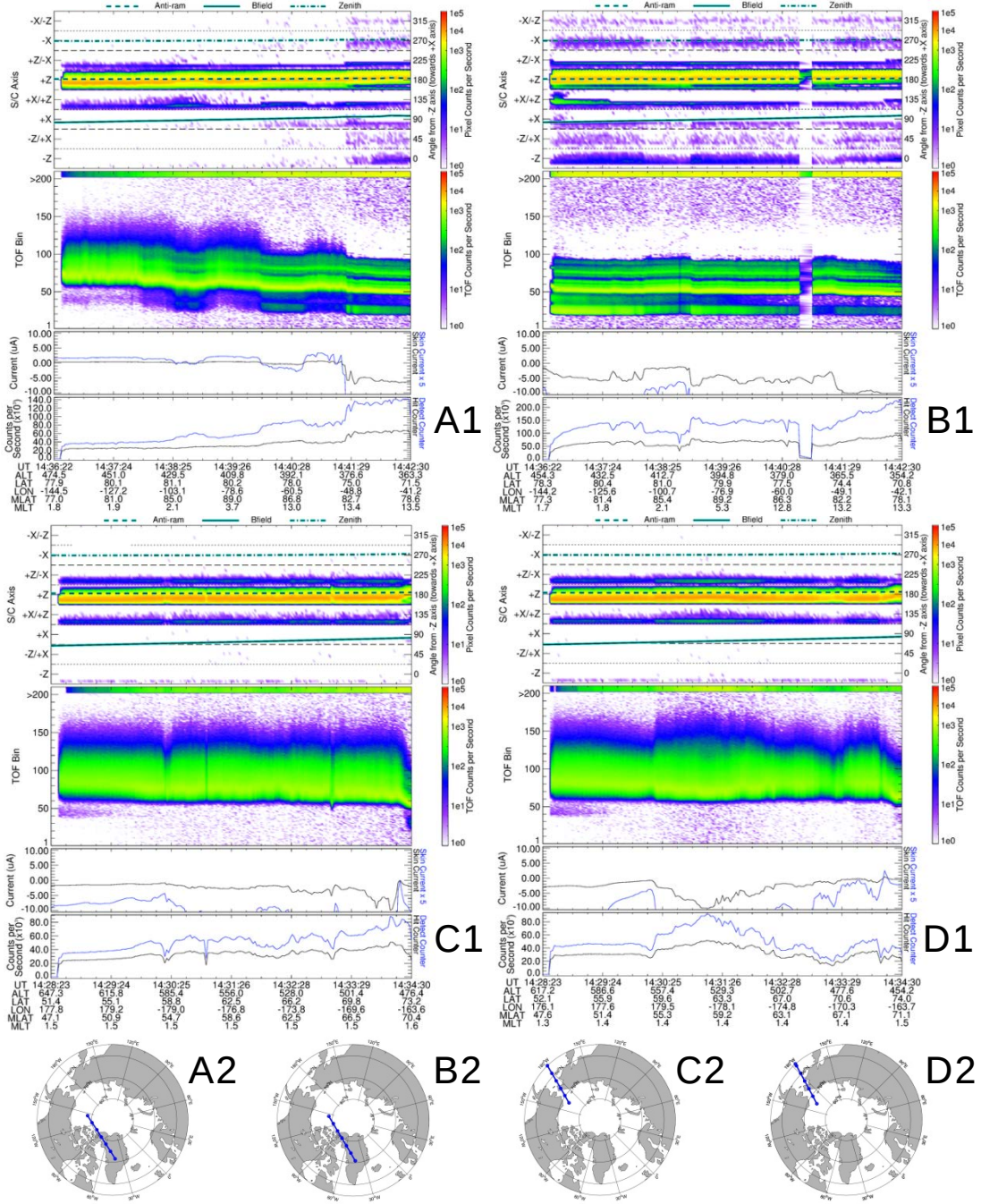

- Time-of-flight versus time (TOF-t) and energy-angle versus time (EA-t) measurements are shown during four different passes.
- **A1** was observed on 17 February, **B1** was on 18 February, **C1** was on 19 February, and **D1** was on 20 February 2014 during near-perigee passes.
- The spacecraft (S/C) Axis panels show the EA-t spectrograms of averaged ion count rate in the order of pixel sectors and pixel radii within the pixel sector.
- The TOF Bin panel shows the TOF-t spectrogram of the ion count rate.

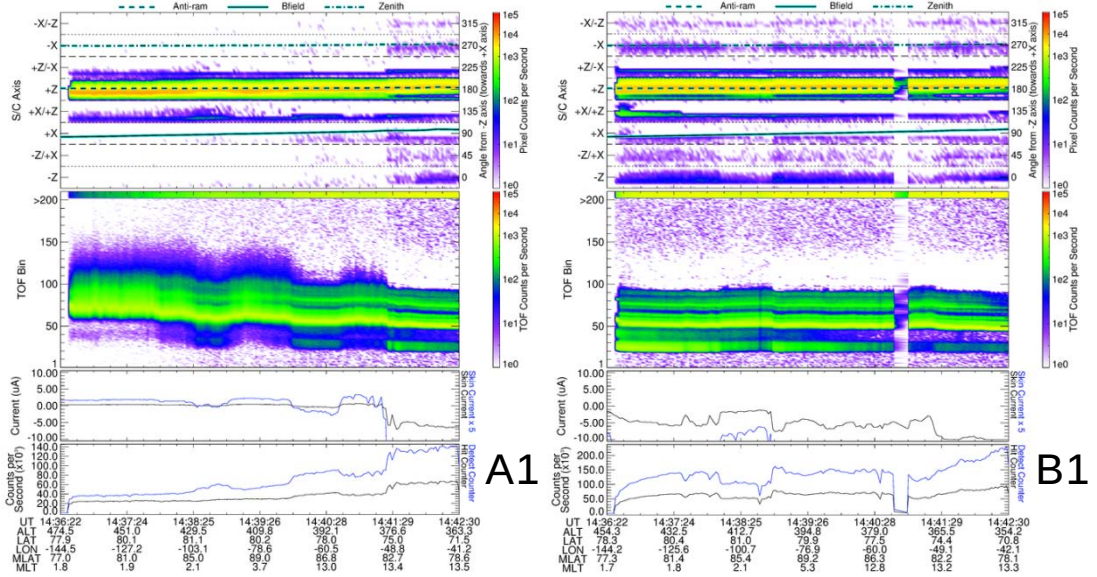

- The TOF bin panels indicate that the satellite encountered more massive species after the storm (**C1** and **D1**) than before (**A1** and **B1**).
- Molecular ion species, such as NO+, are detected at larger TOF bin values [Yau et al., 2015]. These were negligible before the storm day. The main ion drift direction was anti-sunward during each day.
- Weak precipitation was detected before the storm and virtually no ion outflow after the storm. The more massive ion presence in the topside ionosphere after the storm indicates upwelling.

Summary

- GNSS TEC and ionosonde N_e **observations show negative storm effects for several days**. TEC depletion commencements seem to coincide with PCN enhancements.

- We found that the energy input was **mostly a polar-cap phenomenon** (based on PCN changes) and it did not correlate well with Dst and AE indices which began forming disturbances several hours earlier and they would potentially indicate auroral or even lower latitude phenomena.

- During the negative storm phase an atmospheric **negative O/N2 ratio anomaly was observed using GUVI data, which indicated N2 upwelling** and thermospheric wind changes. Ionospheric heating due to the CME's energy input are assumed to initiate these changes in the polar atmosphere.

- Topside sounding of ion densities and velocities using the **IRM sensor showed an increase in heavier ion species during the negative storm phase** that seems to support the suggested heat-induced N2 upwelling mechanism.

- Lastly, our investigations of the ROTI scintillations and comparisons with TEC maps revealed that **strong scintillations mainly resulted from moving patches in the polar cap** while the direct solar ionization does not appear to have had a significant influence.

Acknowledgements

- The authors wish to thank Lowell Digisonde International for providing access to Thule Digisonde data used in this work; the Greenland GPS Network (GNET) operated by the Technical University of Denmark, National Space Institute (DTU Space) in cooperation with the American National Science Foundation, Ohio State University, and the non-profit university governed consortium UNAVCO for GPS data; the Technical University of Denmark, National Space Institute's Geomagnetism Section for magnetometer observations; and NASA Jet Propulsion Laboratory for GIM data processing.

- The GUVI data used here were provided through support from the NASA Mission Operations and Data Analysis program. The GUVI instrument was designed and built by The Aerospace Corporation and The Johns Hopkins University. The principal investigator is Dr. Andrew B. Christensen and the chief scientist and co-PI is Dr. Larry J. Paxton.

- The authors also acknowledge the use of SuperDARN convection data and CASSIOPE IRM sensor data from e-POP.

- Richard Langley acknowledges funding support from the Natural Sciences and Engineering Research Council of Canada and the Canadian Space Agency.

- Data used in this paper can be obtained from the authors.

References

Basu, S., S. Basu, E. MacKenzie, and H. E. Whitney (1985), Morphology of phase and intensity scintillations in the auroral oval and polar cap, Radio Sci., 20(3), 347–356, doi:10.1029/RS020i003p00347.

Gherm, V. E., and N. N. Zernov (1995), Fresnel filtering in HF ionospheric reflection channel, Radio Sci., 30(1), 127–134, doi:10.1029/94RS01035.

Kersley, L., S. E. Pryse, and N. S. Wheadon (1988), Amplitude and phase scintillation at high latitudes over northern Europe, Radio Sci., 23(3), 320–330, doi:10.1029/RS023i003p00320.

Pi, X., A. J. Mannucci, B. Valant-Spaight, Y. Bar-Sever, L. J. Romans, S. Skone, L. Sparks, and G. Martin Hall (2013), Observations of Global and Regional Ionospheric Irregularities and Scintillation Using GNSS Tracking Networks, Proceedings of the ION 2013 Pacific PNT Meeting, Honolulu, Hawaii, April 2013, pp. 752-761.

Yeh, K. C. and C-H. Liu (1982), Radio wave scintillations in the ionosphere, Proceedings of the IEEE, 70, 4, pp. 324 – 360, 10.1109/PROC.1982.12313.

Instruments and Techniques
Greenlandic Geomagnetic Observatories

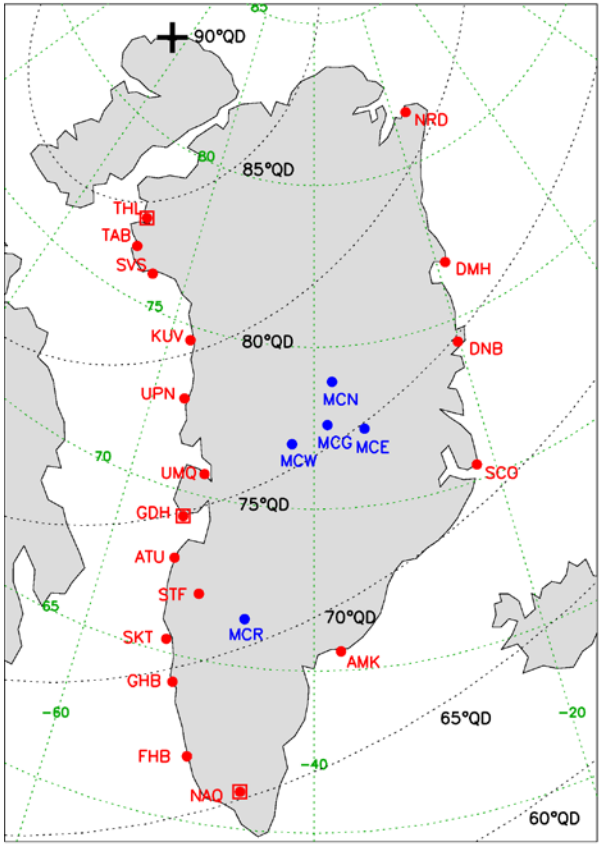

Magnetic observatory

Variometer station

Variometer station (MAGIC)

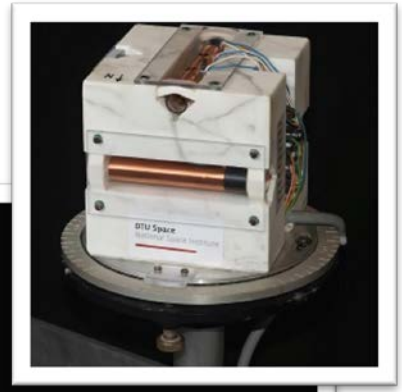

Results – Local Magnetic Measurements

- 1 Hz vector variometer measurements from Greenlandic ground-stations of the magnetic field vector north component on 19 February 2014. Thule is the northernmost and Nuuk is the southernmost station among the three indicated in the figure.

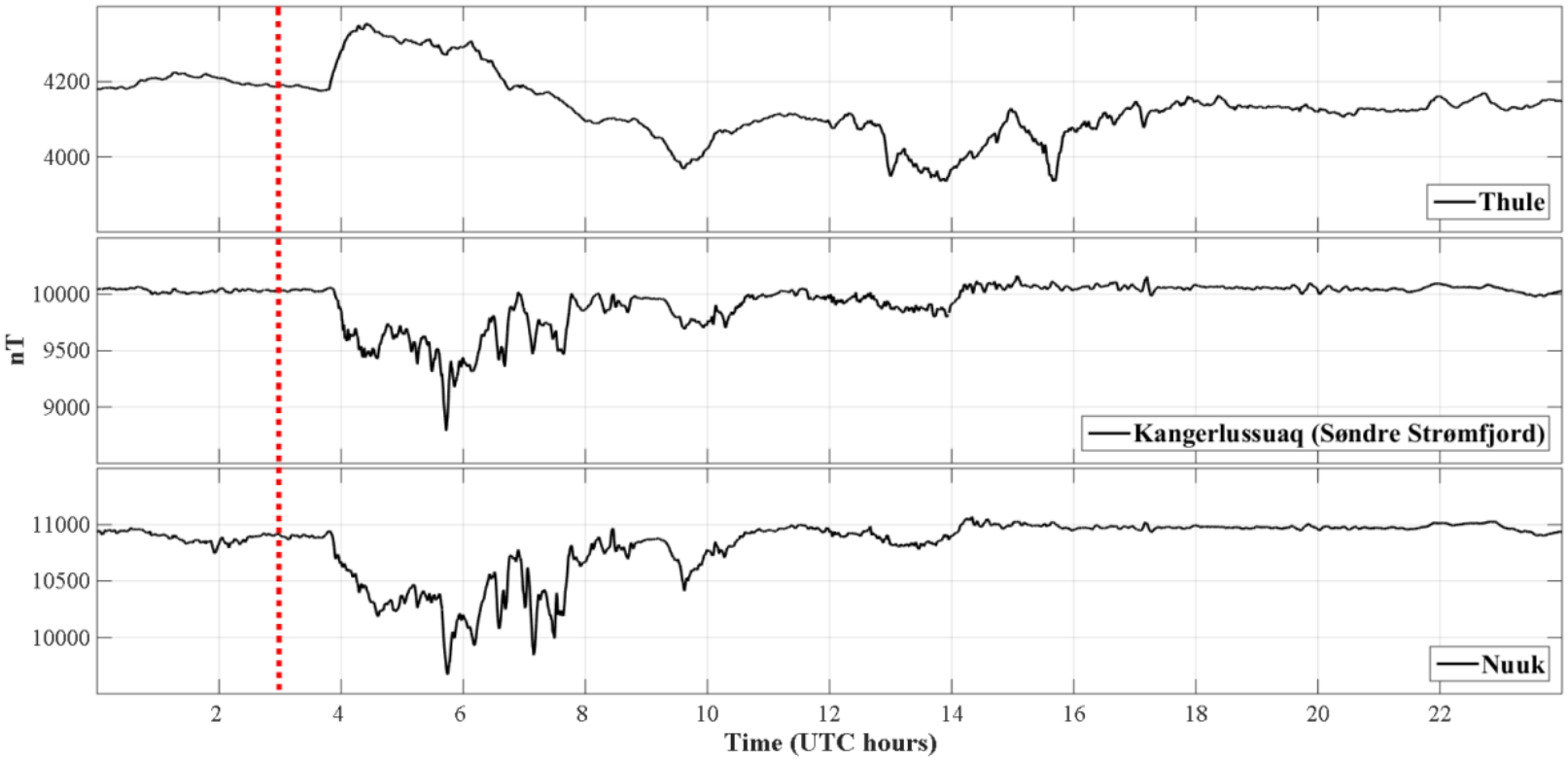

Results – SuperDARN vs. VTEC

- 2014 February 19 Geomagnetic Storm - VTEC

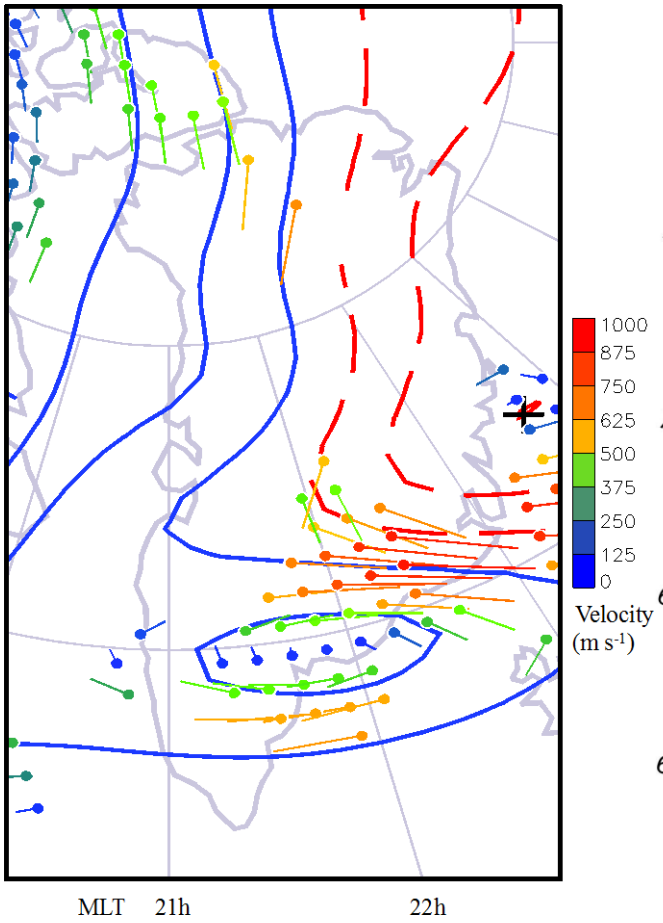

SuperDARN convection map

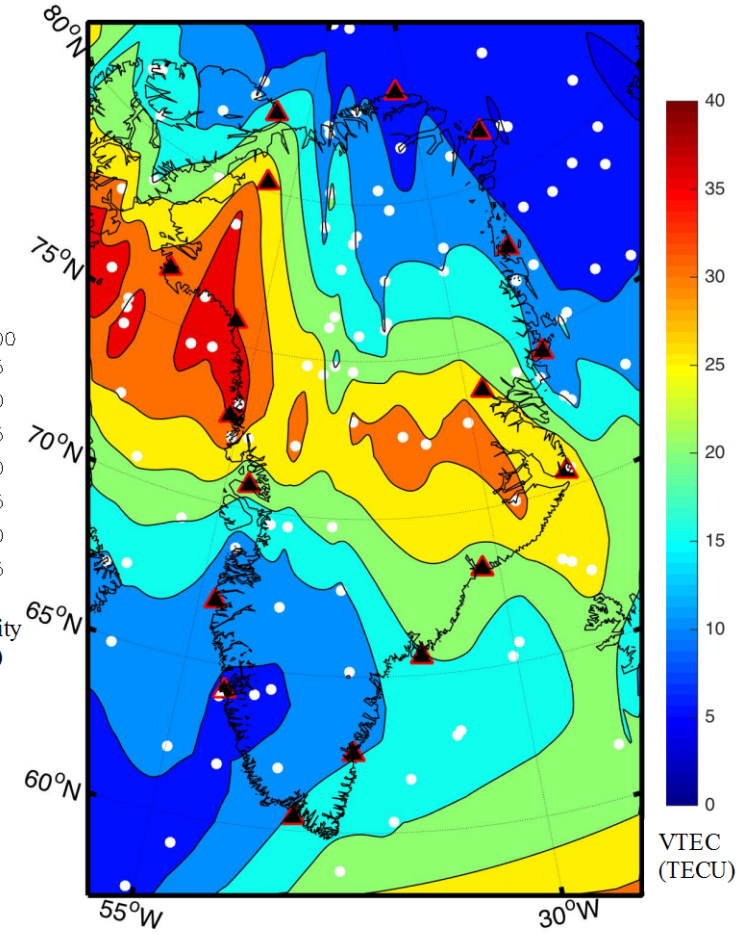

VTEC map over Greenland

Results - GUVI

- Longitudinal profiles demonstrating O/N_2 ratios (unitless) along 73-degree north latitude. The first CME hit on 19 February and the second on 20 February.